Supplemental Material

Influences of polarity and hydration cycles on imbibition hysteresis in silica nanochannels

Shaina Kelly, Carlos Torres-Verdín, and Mathew Balhoff

Department of Petroleum and Geosystems Engineering, The University of Texas at Austin, Austin, TX 78712
Center for Nano- and Molecular Science, The University of Texas at Austin, Austin, TX, 78712

Supplemental Material 1: Tables of experimental conditions

Table SM1. Chip A (IPA-water)

Test #	Δt_{dry} (s)	T (°C)	P (torr)
1	2280	150	510
2	61200	190	380
3	300	190	380
4	71100	190	380
5	1740	190	380
6	72240	190	380
7	960	190	200
8	2592000	25	760
9	14820	270	200
10	60900	270	200
11	77640	270	200
12	448200	25	760
13	2940	280	180
14*	169200	25	8274 kPa
15**	3180	280	180
16	67320	280	180

* Critical point drying

**Calibration heptane experiment

Table SM2. Chip B (Heptane)

Test #	Δt_{dry} (s)	T (°C)	P (torr)
1	0	25	760
2	58620	270	200
3	77640	270	200
4	720	270	200
5	2940	270	180
6	252000	25	760
7	840	280	180
8*	110640	280	180

* Calibration IPA-water experiment

Recall, 0 torr is a perfect vacuum and 760 torr is atmospheric pressure. Torr is equivalent to mm Hg absolute pressure.

Supplemental Material 2: Poiseuille solution for a rectangular channel

The Poiseuille flow analytical solution for the permeability of a rectangular conduit [1] of depth *d* and width *w*, similar to the trapezoidal nanochannels of this work, is

$$k_r = \frac{d^2}{12}\left[1 - \sum_{n,odd}^{\infty} \frac{1}{n^5}\frac{192}{\pi^5}\frac{d}{w}\tanh\left(n\pi\frac{w}{2d}\right)\right] . \qquad \text{* MERGEFORMAT (1)}$$

If hydration films coat the corners of a rectangular nanochannel and are immobile then the Poiseuille equation for an elliptical cross-section of major and minor axes *w* and *d* may be appropriate [1]:

$$k_e = \frac{1}{4}\frac{(wd)^2}{w^2 + d^2} . \qquad \text{* MERGEFORMAT (2)}$$

For the same *d* and *w* the permeability of an elliptical cross-section is roughly half that of a rectangular cross-section.

Supplemental Material 3: Channel size effects

The effect of channel size on liquid uptake results was not apparent as a dominant control for the given range of nanochannel sizes.

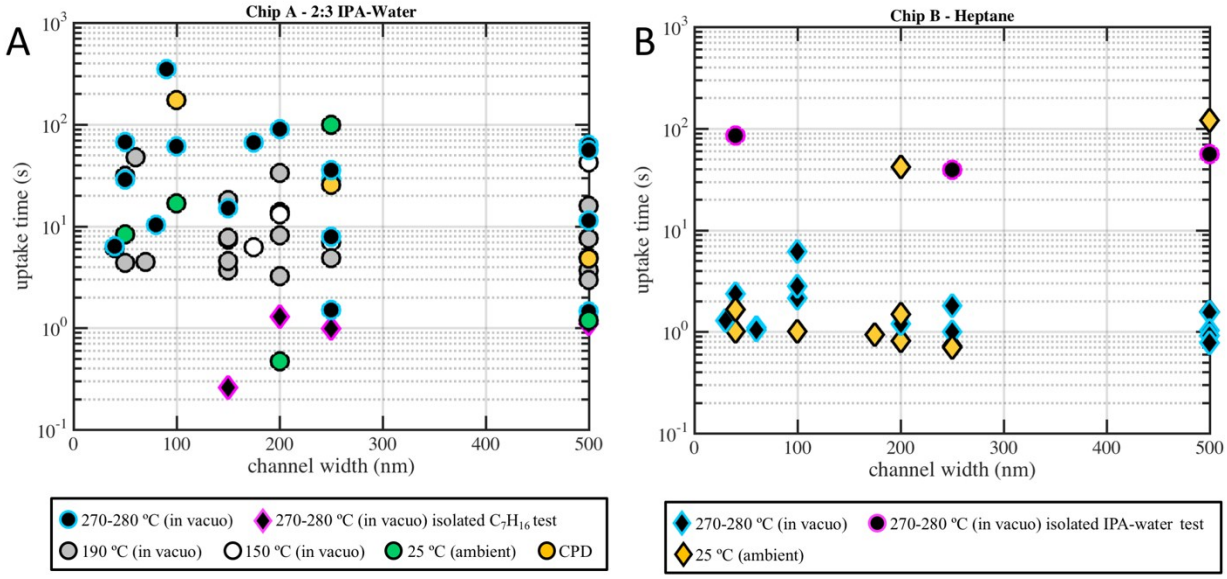

FIG. SM1. Uptake time, the amount of time it takes to fill the 250 μm long nanochannels is plotted versus nanochannel width for (A) Chip A and (B) Chip B. The channels are all 60 nm in height.

<u>Supplemental Material 4.A</u>: Log-log plots of imbibition data

Below are the log-log plot versions of the manuscript's Figure 4. **Data curves that do not fit to power-law trends are nonlinear in the log-log plots.** The differences in n-values are accentuated by log-log plots because the slope of the trends is equal to n. Pale solid background curves in the three plots indicate $n = 0.5$ power-law trends for arbitrary α-values in $l(t) = \alpha t^n$, which can be referenced to clarify the goodness (or poorness) of fit of the data to Lucas-Washburn dynamics.

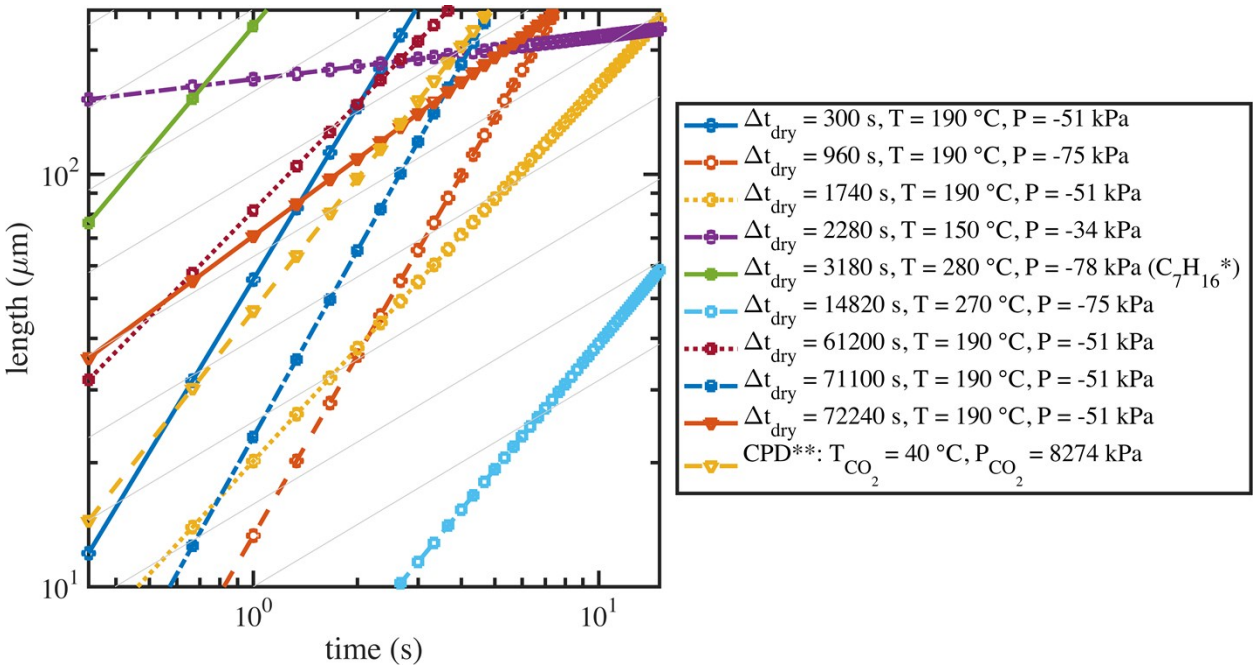

FIG. SM2. Log-log plot of 2:3 IPA:DI water imbibition in a 500 nm × 60 nm glass-silica nanochannel for varying pressure, temperature, and length of drying conditions. Vacuum pressures are given as negative gauge pressures where the zero reference is atmospheric pressure (101 kPa). The positive pressure values are absolute pressures.

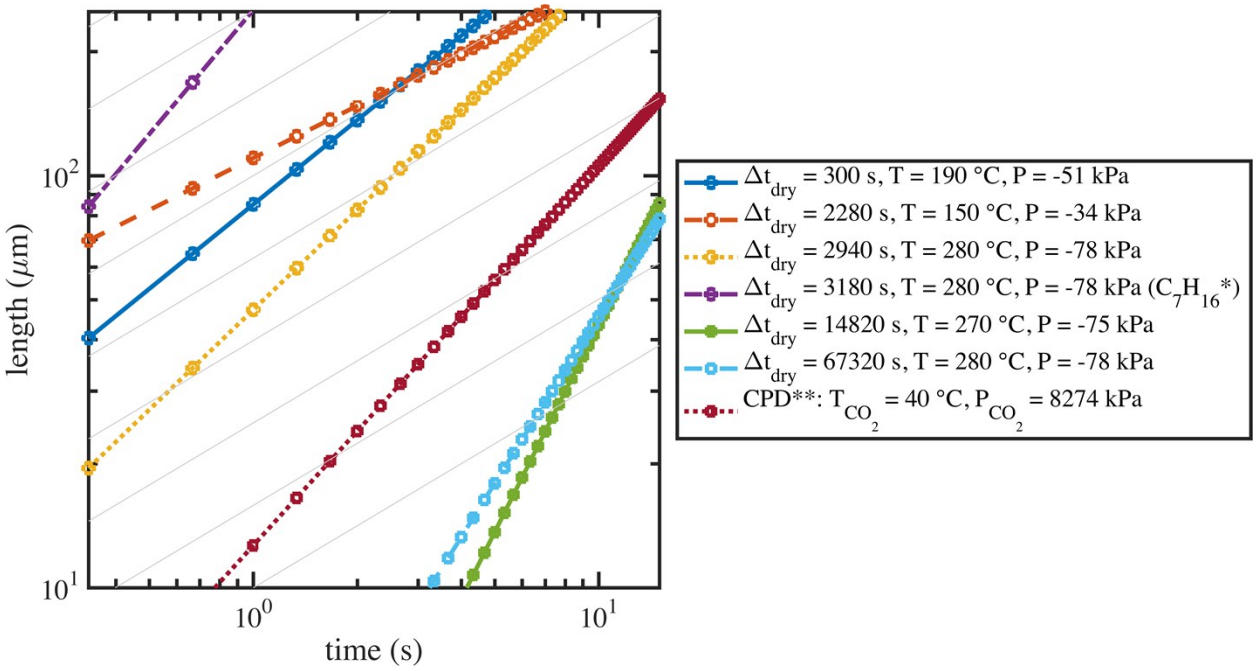

FIG. SM3. Log-log plot of 2:3 IPA:DI water imbibition in a 250 nm × 60 nm glass-silica nanochannel for varying pressure, temperature, and length of drying conditions. Vacuum pressures are given as negative gauge pressures where the zero reference is atmospheric pressure (101 kPa). The positive pressure values are absolute pressures.

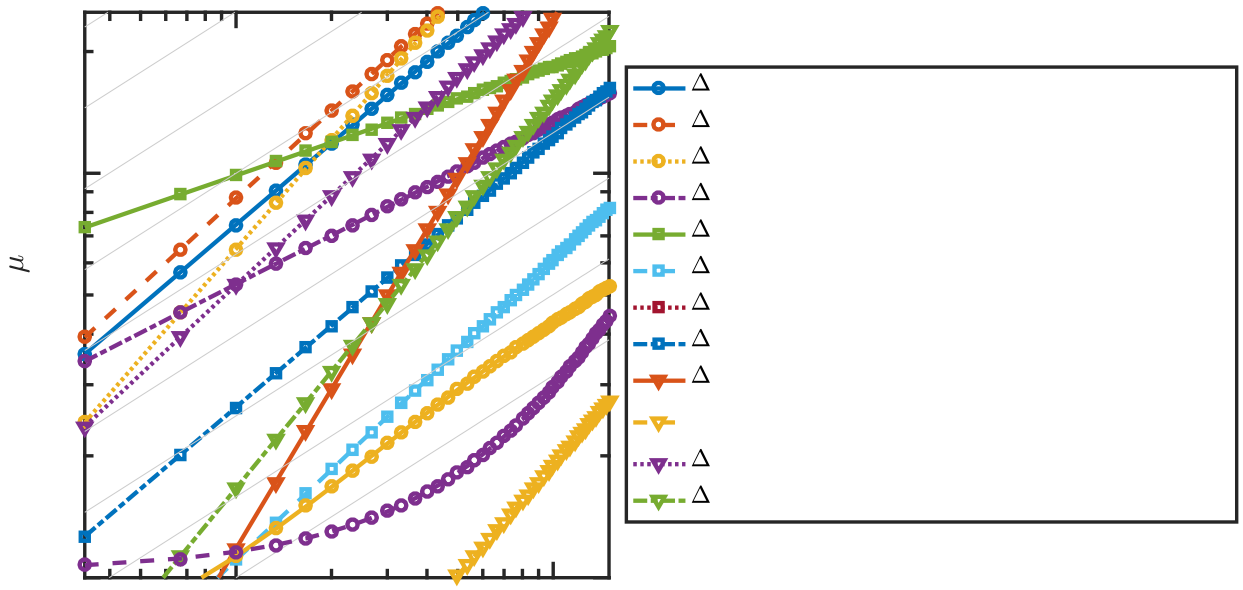

FIG. SM4. Log-log plot of 2:3 IPA:DI Water imbibition in glass-silica nanochannels smaller than or equal to dimensions of 100 nm × 60 nm for varying pressure, temperature, and length of drying conditions. Vacuum pressures are given as negative gauge pressures where the zero reference is atmospheric pressure (101 kPa). The positive pressure values are absolute pressures.

<u>Supplemental Material 4B</u>: Plots of imbibition data for additional channel sizes

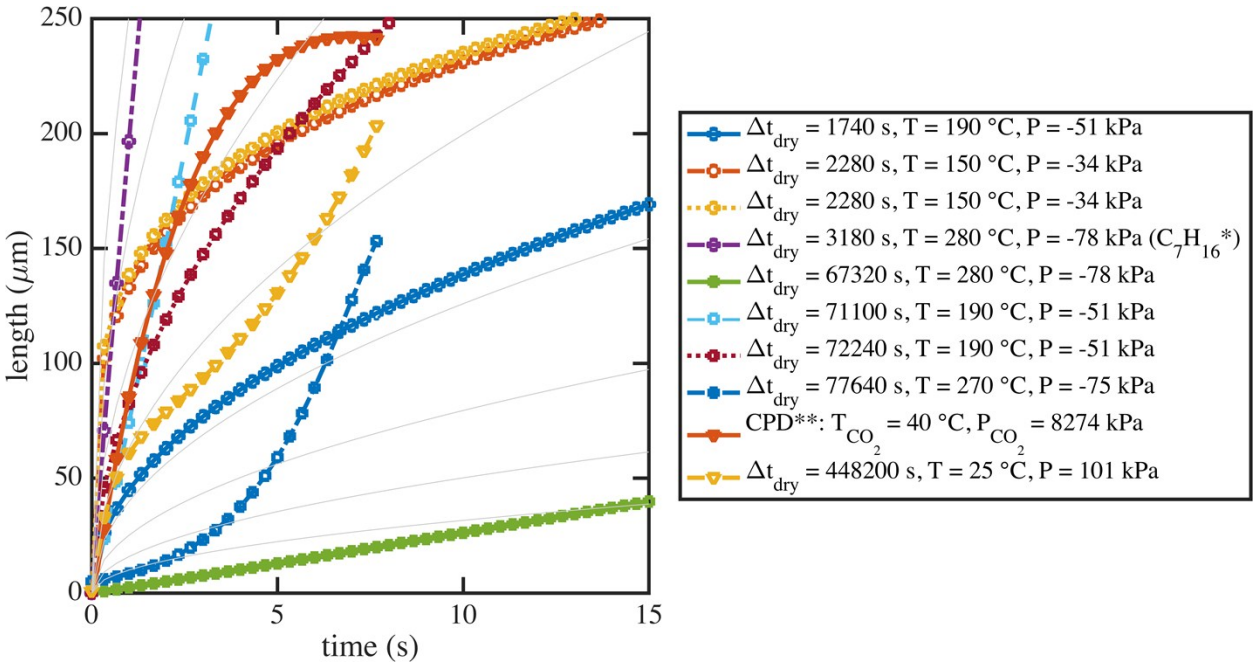

FIG. SM5. Plot of 2:3 IPA:DI water imbibition in 200 nm × 60 nm glass-silica nanochannels for varying pressure, temperature, and length of drying conditions.

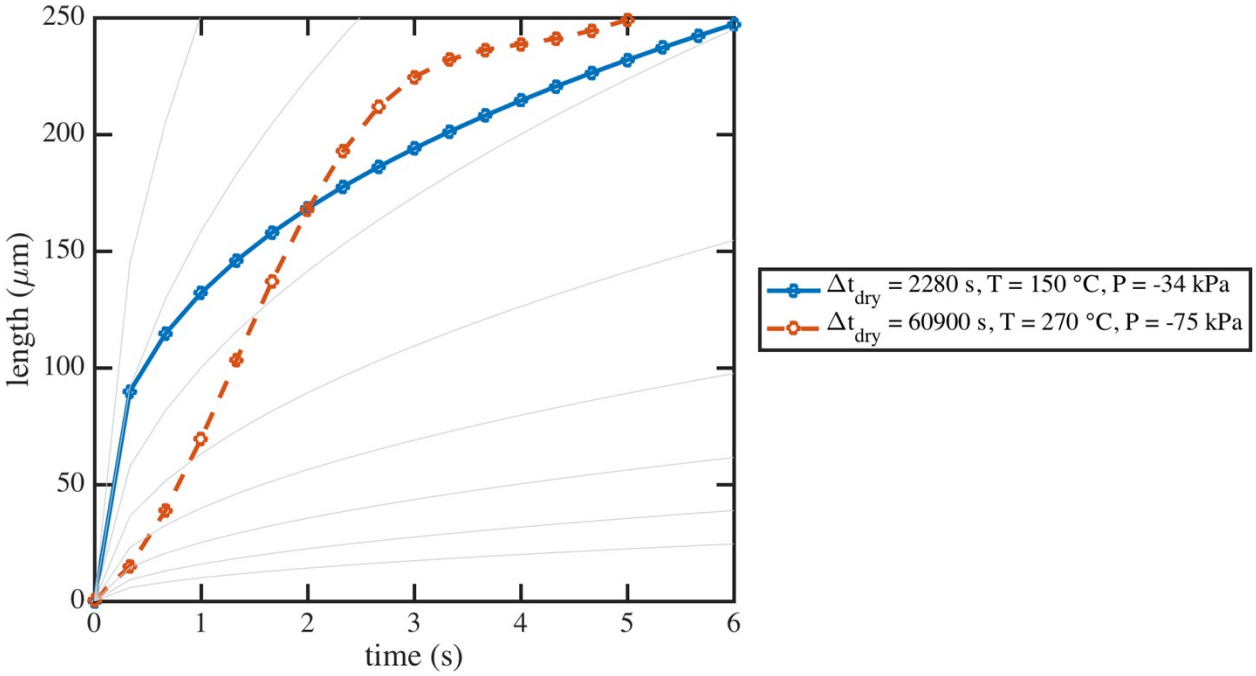

FIG. SM6. Plot of 2:3 IPA:DI water imbibition in 175 nm × 60 nm glass-silica nanochannels for varying pressure, temperature, and length of drying conditions.

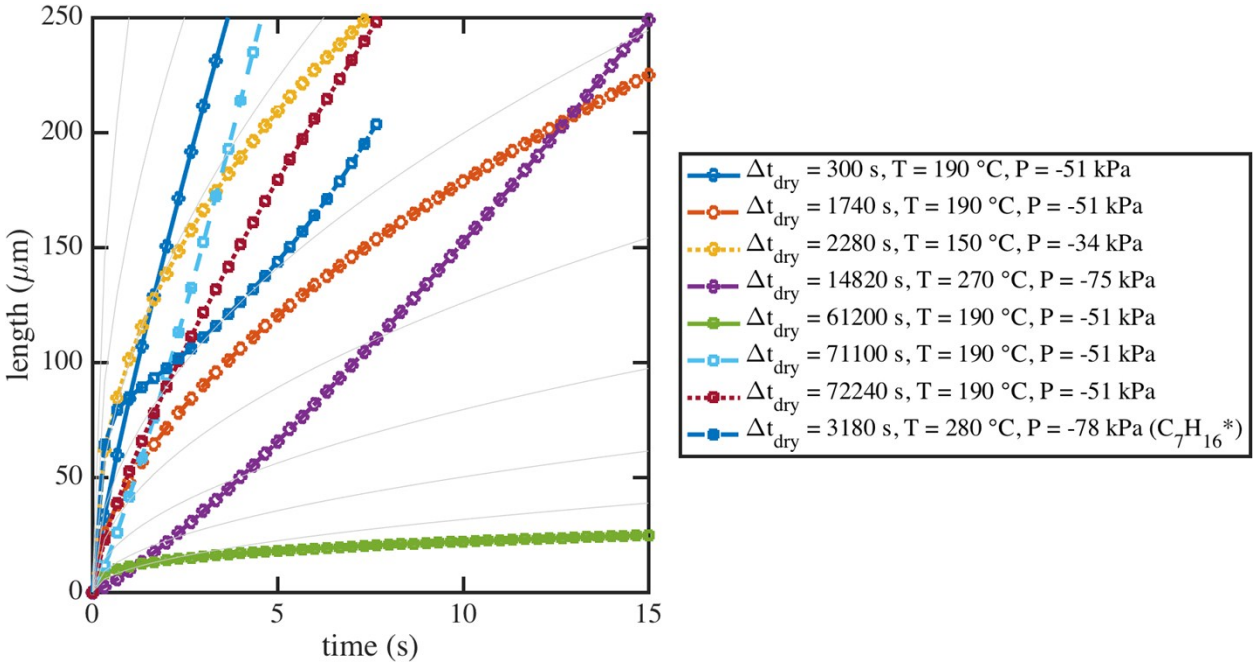

FIG. SM7. Plot of 2:3 IPA:DI water imbibition in 150 nm × 60 nm glass-silica nanochannels for varying pressure, temperature, and length of drying conditions.

Supplemental Material 5: IPA imbibition captured at a rapid frame rate

Imbibition of pure isopropanol (IPA) in a nanofluidic chip (from the same fabrication batch as Chips A and B featured in the manuscript) was captured with an inverted Nikon Ti microscope (reflected DIC microscopy mode) and a CCD camera frame rate of ~ 21 fps. The chip was only exposed to IPA and was subject to 24 hours of air drying [from the previous IPA exposure] before the imbibition experiment shown in Figure SM8. Prior to pipetting liquid at the chip inlet, no liquid plugs were observed in the nanochannels. Figure SM8 displays examples of the dynamic imbibition data for several nanochannel sizes.

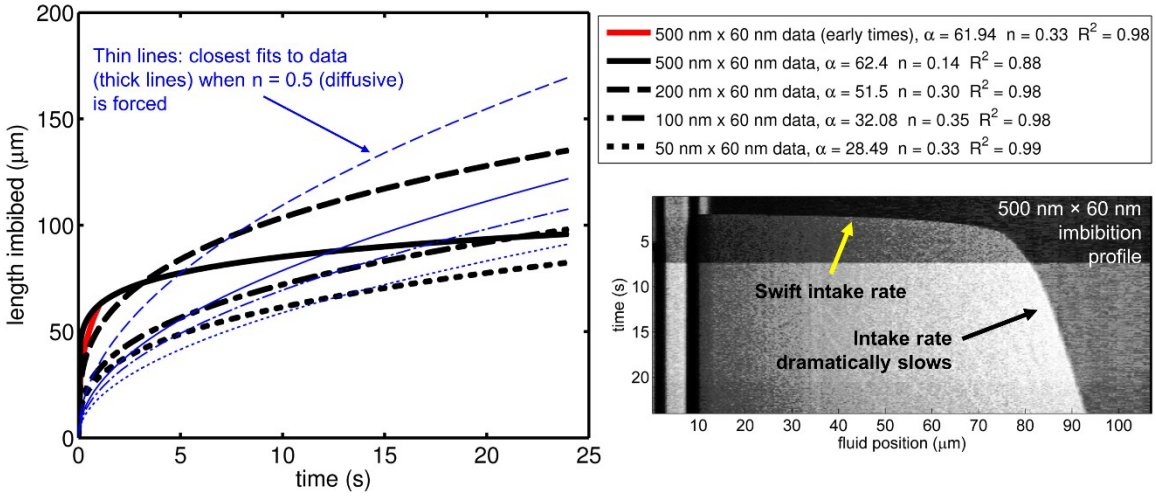

FIG. SM8. IPA imbibition data (captured at 21 frames per second) that exhibits a swift intake rate followed by a dramatic slowdown; i.e. $n < 0.5$. Data α and n fits for several channels are given in the figure key. Thin blue lines represent forced fits of $n = 0.5$ for comparison purposes. The right inset is an example imbibition profile from the raw stack of DIC images that corresponds to the solid red and black lines in the imbibition plot.

Imbibition fronts moved swiftly at early times, but then dramatically slowed down and, in some cases, fontal motion became arrested. In these later times, the meniscus appeared to "struggle" in a stick-slip fashion. For t^n power laws fit to the entirety of the imbibition data, such a trend corresponds to $n < 0.5$; n was found to typically be ~ 0.3 for these scenarios (see n-values in the legend in Figure SM8). When IPA imbibition experiments were performed in the same chip at a later date and after a longer period of air drying, imbibition was faster and exhibited different non-Washburn power law values; for instance, the 500 nm x 60 nm channel imbibed linearly.

Supplemental Material 6: Extracting channel profiles from imbibition data

Shape variation or variation in effective channel cross section along sufficiently long channels results in non-diffusive imbibition [2]. For cylinders, analytical solutions for imbibition in channels of non-constant cross-sections of monotonic variation are polynomial relationships; at late times in both axially divergent and convergent channels $t^{1/3}$ and $t^{1/4}$ power laws were found for, respectively, 2D (slit) and 3D (channel) cases [2] [3]. Per the coefficients in these solutions, imbibition is predicted to be faster in convergent

channels than the Washburn equation for a consistent cross-section and vice versa for diverging channels; such relative speeds hinge upon adherence to the Young-Laplace equation.

An unknown variation in channel radius or effective channel radius, *r(x)*, can be determined from the curve of experimental imbibition velocity data by an inverse problem method [4]. The radius of the channel at a specific position, $r(l_0)$, must be known for this method to render a unique solution. In the case of narrow channels with bound hydration films, we suggest the assumption that film evaporation is most complete at the mouths/endpoints of the nanochannels; accordingly, $r(0)$ or $r(L)$ is approximately the fabricated radius (or hydraulic radius) of the nanochannel. For a cylindrical channel, Elizalde et al. [1] derive the variation in channel size at imbibition length $r(l)$ from

$$u = \frac{dl}{dt} = \frac{\gamma \cos\theta}{\mu}\left[4r(l)^3 \int_0^l \frac{dx}{r(x)^4} \right]^{-1}, \tag{4}$$

and arrive at

$$r(l) = \left[r(l_0)u(l_0)^{1/3} + \frac{4}{3\alpha}\int_l^{l_0} u(l)^{4/3}\, dl \right] u(l)^{-1/3} \ . \tag{5}$$

A rectangular channel with thin films and bound liquid regions in the corners can be represented by an ellipse. A circle is just a special case of the Poiseuille equation for an elliptical cross-section of major and minor axes a and b [1]:

$$u = \frac{1}{4}\frac{(ab)^2}{a^2+b^2}\frac{\Delta P}{\mu L} \ . \tag{6}$$

For an elliptical channel with non-constant cross-section,

$$u(l) = \frac{dl}{dt} = \frac{\gamma \cos\theta}{2\mu}\left(\frac{1}{a(l)^2 b(l)} + \frac{1}{a(l)b(l)^2} \right)\left[\int_0^l \frac{a(x)^2 + b(x)^2}{a(x)^2 b(x)^2} \right]^{-1} \ . \tag{7}$$

Eq. 7 can be used to solve for $r(l)$ in a channel with elliptical cross sections.

References

[1] H. Bruus, *Theoretical Microfluidics* (OUP Oxford, 2008).

[2] M. Reyssat, L. Courbin, E. Reyssat, and H. A. Stone, Imbibition in Geometries with Axial Variations, J. Fluid Mech. **615**, 335 (2008).

[3] D. Losic and A. Santos, *Nanoporous Alumina: Fabrication, Structure, Properties and Applications* (Springer, 2015).

[4] E. Elizalde, R. Urteaga, R. R. Koropecki, and C. L. A. Berli, Inverse Problem of Capillary Filling, Phys. Rev. Lett. **112**, 134502 (2014).